

HEATING IN AN EXTENDED ACCRETION DISK CORONA ALONG THE Z-PATTERN IN CYG X-2

N. S. SCHULZ¹, D. P. HUENEMOERDER¹, L. JI¹, M. NOWAK¹, Y. YAO², AND C. R. CANIZARES¹

Submitted for publication to The Astrophysical Journal

ABSTRACT

We observed at very high spectral resolution the prototype Z-source Cyg X-2 twice along its entire X-ray spectral variation pattern. In this preliminary analysis we find an extended accretion disk corona exhibiting Lyman α emissions from various H-like ions, as well as emissions from He-like ions of Fe and Al, and Be-like ions of Fe. The brightest lines show a range of line broadening: H-like lines are very broad with Doppler velocities between 1100 and 2700 km s⁻¹, while some others are narrower with widths of a few hundred km s⁻¹. Line diagnostics allow us for the first time to determine coronal parameters. The line properties are consistent with a stationary, extended up to 10¹⁰ cm, dense (1×10^{15} cm⁻³), and hot ($\log \xi \gtrsim 3$; $T \gtrsim 10^6$ K) accretion disk corona. We find ongoing heating of the corona along the Z-track and determine that heating luminosities change from about $0.4 \times L_{\text{Edd}}$ on the horizontal to about $1.4 \times L_{\text{Edd}}$ on the flaring branch.

Subject headings: stars: individual (Cyg X-2) — stars: neutron — X-rays: stars — binaries: close — accretion: accretion disks — techniques: spectroscopic

1. INTRODUCTION

At the end of the 1980s two classes of Low-Mass X-ray Binaries (LMXBs) emerged based on their behavior with respect to X-ray luminosity, spectral, and timing evolution (Hasinger & van der Klis 1989). Bright LMXBs with luminosities near the Eddington luminosity L_{edd} show spectral variations in the color-color diagram (CD) where the spectral slope and normalization evolve in a continuous pattern from a horizontal branch (HB) to a normal branch (NB) to a flaring branch (FB) and back (Schulz, Hasinger & Trümper 1989). Multi-wavelength studies in the case of the prototype Z-source Cyg X-2 have indicated that mass accretion rate seems to continuously change along the Z-track (Hasinger et al. 1990; O’Brien et al. 2004). The source itself has an estimated distance of 8–11 kpc (Cowley et al. 1979; Smale 1998), its companion is an evolved star of a mass ranging between 0.4 and 0.7 M_{\odot} . The source has been known to show extensive dipping activity on the FB, which leads to estimated angle of inclination of at least 60°. It has long been speculated that intensity and spectral changes are a consequence changes in geometrical and optical thickness of the accretion disk and possibly an associated accretion disk corona (Vrtilek et al. 1988; ADC). It is also well established that bright LMXBs show Fe K α emissions (White et al. 1985, 1986; Hirano et al. 1987), which in the case of Cyg X-2 have been identified with He-like Fe XXV at 6.71 keV using the higher resolution spectrometer onboard *BBXRT* (Smale et al. 1994). Subsequent observations with *ASCA* detected an additional broad emission line complex around 1 keV, while observations with *BeppoSAX* introduced additional line detections consistent with Fe XXIV, Si XIV, and S XVI, with fairly narrow claimed equivalent widths (Smale et al. 1994; Kuulkers et al. 1997). The most thorough spectral analysis of Cyg X-2 spectra along the Z-spectral pattern was performed by Di Salvo et al. (2002), and to date the most consistent line detections concern the broad emission line features at 1 keV and at 6.6–6.7 keV. Thus although the existence of line emis-

sion in Cyg X-2 is now fairly established, basic line properties, i.e. precise positions, widths, and fluxes, remain undetermined. Furthermore, since the Z-shaped spectral changes in the color-color diagram were discovered, there has been little progress in understanding this pattern.

TABLE 1: OBSERVATIONS IN 2007

Obsid	Start Date [UT]	Start Time [UT]	Exp. [ks]	HETG 1st cts s ⁻¹
8170	Aug 25 2007	17:45:20	70.2	272.23
8599	Aug 23 2007	05:02:33	64.4	276.31

Chandra observations of Z-sources to date so far have only been confirmed in Cir X-1 (Brandt & Schulz 2000; Schulz et al. 2008). In this letter we report on the detection of broad and highly ionized emission lines in a recent long exposure of Cyg X-2 with *Chandra*, which allows the precise determination of line positions, line widths, and line fluxes. We also report on the first detection of a strong line flux correlation with the Z-pattern in Cyg X-2.

2. CHANDRA OBSERVATIONS

Cyg X-2 was observed with the High Energy Transmission Grating Spectrometer (HETGS, see Canizares et al. 2005 for a detailed description) on 2007 August 25 (starting at 17:45:20 UT) for 70.2 ks (OBSID 8170, obs. 1) and on 2007 August 23 (starting at 05:02:33 UT) for another 64.4 ks (OBSID 8599, obs. 2). The X-ray source is one of the brightest in the sky, the ASM onboard the *Ross X-Ray Timing Explorer* (*RXTE*) recorded an average of about 0.484 Crab throughout 2005, Given *Chandra*’s enormous spatial resolution, the fastest available detector readout time (3.82 msec), as provided in continuous clocking (CC) mode in order to mitigate pileup in the grating spectra, was chosen. Table 1 summarizes basic observational parameters.

¹ Kavli Institute for Astrophysics and Space Research, Massachusetts Institute of Technology, Cambridge, MA 02139.

² CASA, University of Colorado, Boulder, CO.

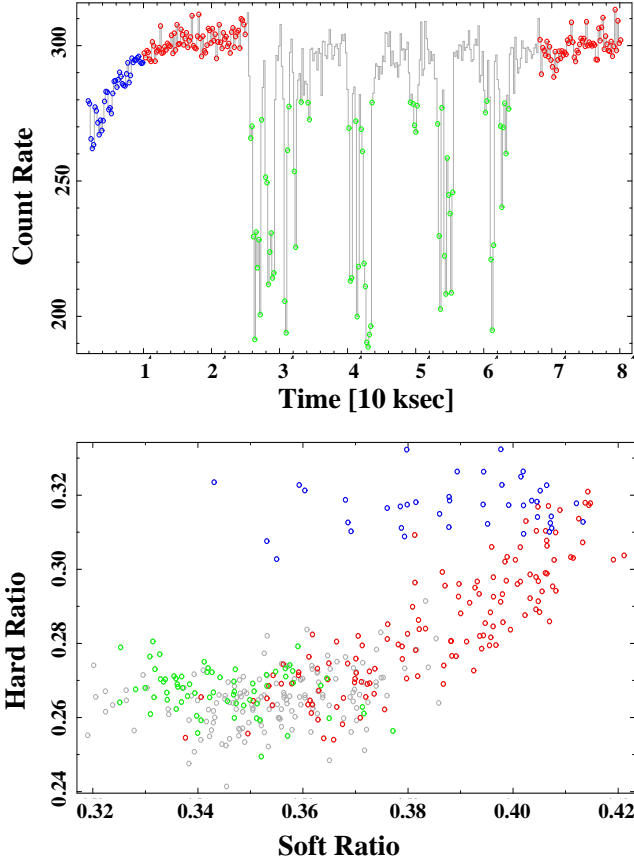


FIG. 1.— **Top:** The light curve of observation 1. The colors correspond to the spectral branches in the color-color diagram with HB (blue), NB (red), and FB (green (dip) & grey (non-dip)). **Bottom:** The color-color diagram of the lightcurve above.

All data were reprocessed using CIAO4.0 and the most recent CALDB products. The first order count rates of ~ 270 cts s^{-1} were quite similar during both observations and correspond to an average value for the cts/frame/node of ~ 0.04 and we do not worry about pileup. The calibration with respect to charge transfer inefficiency (CTI) in timed exposure (TE) mode cannot be used for CC mode, as here the short clocking time changes the charge trap pattern in the device slightly reducing the effects of CTI. Although the fast clocking limits CTI, we must manually adjust the order sorting tables to capture trailing charges. Additionally, the continuous clocking morphs some of the flight event grades into flight grades outside the telemetered standard grade system. The result is a continuous decrease in effective area towards higher energies. In contrast to the effects of pileup, however, discrete line features remain preserved.

For the purpose of this letter we actually do not need the most precise area calibration as we are not fitting physical continuum models. To fit emission lines we used the interactive analysis software ISIS³ (Houck & Denicola 2000), applied standard wavelength redistribution matrix files (RMF), and generated standard ancillary response files (ARFs)⁴. For all the observations we generated spectra and analysis products for the 1st orders only. We co-add ± 1 st orders of both gratings, which results in a spectral grid of close to

0.021 \AA and an average of several $\sim 10^4$ cts bin^{-1} between 1.8 and 14 \AA . For the spectral analysis we always co-add both observations. We determine an unabsorbed (Juett et al. 2004) source flux in the HETG spectra of $(1.53 \pm 0.25) \times 10^{-8} \text{ erg cm}^{-2} \text{ s}^{-1}$.

3. LIGHT CURVES AND COLOR-COLOR DIAGRAMS

The top panel in Figure 1 shows the light curve of obs. 1, the one in obs. 2 is very similar. The source was so strong that many frames were dropped during transmission. In order to properly deal with this effect we employed the “aglc” package which is contributed software linked to from the CIAO pages⁵. Frame drops vary between 10% and 70% in single CCDs at a time.

Both light curves appear morphologically very similar and feature a steady rise, periods of steady high flux, and various rapid dipping periods. The HETG count rate varies between 200 and 300 cts s^{-1} amounting to an equivalent of 0.47 Crab on average. Bins of 500 s thus result in very small statistical uncertainties. Due to the limited bandpass in the HETGS we have use slightly different wavelength bands to compute hardness ratios with respect to studies done with EXOSAT, GINGA, and RXTE. We chose $f_{xs} = \text{flux}(0.5 \text{ keV} - 2.5 \text{ keV})$, $f_{xm} = \text{flux}(2.5 \text{ keV} - 4.5 \text{ keV})$, and $f_{xh} = \text{flux}(4.5 - 8.0 \text{ keV})$ and thus for the hard ratio f_{xh}/f_{xm} and the soft ratio f_{xm}/f_{xs} .

TABLE 2: X-RAY LINE PROPERTIES

ion	λ_{meas} \AA	Flux _{line} (a)	v_D km s^{-1}
Fe XXVI	1.792 ± 0.009	0.39 ± 0.28	1120 ± 870
Fe XXV	1.861 ± 0.005	1.97 ± 0.27	3450 ± 710
S XVI $L\alpha$	4.726 ± 0.011	0.79 ± 0.25	1860 ± 1140
Si XIV $L\alpha$	6.188 ± 0.005	1.03 ± 0.15	1610 ± 290
Al XII	7.812 ± 0.003	0.38 ± 0.06	530 ± 110
Fe XXIV	7.973 ± 0.001	0.78 ± 0.05	370 ± 40
Mg XII $L\alpha$	8.419 ± 0.004	1.26 ± 0.38	2730 ± 480
Ne X $L\alpha$	12.13	$\lesssim 1.3$	$\lesssim 5600$

(a) $10^{-4} \text{ ph s}^{-1} \text{ cm}^{-2}$, uncertainties are 90% confidence

The color-color diagram corresponding to the light curve of obs. 1 is shown at the bottom of Figure 1. In each of the two observations the entire Z-track is covered once. The hardness variability behavior follows the established pattern seen in Cyg X-2 in recent years with HB and NB corresponding to flux rise and stability and the FB corresponding to dipping.

4. THE PROPERTIES OF BRIGHT EMISSION LINES

The unfolded flux spectrum in the range between 1.5 and 25 \AA exhibits a variety of line features. These consist of narrow absorption lines at longer wavelengths and broad emission lines at shorter wavelength. The line absorption is attributed to the interstellar medium will be dealt with in a separate paper (Yao et al. 2008). In this letter we focus entirely on the measurement of a few of the isolated and brightest emission lines at short wavelengths ($< 14 \text{ \AA}$). These lines are well

³ see <http://space.mit.edu/ASC/ISIS/>

⁴ see <http://asc.harvard.edu/ciao/threads/>

⁵ see <http://asc.harvard.edu/ciao/download/scripts/>

resolved with respect to the instrument resolution, which allows us to determine excess fluxes independent of the underlying continuum and thus for the first time provide a direct diagnostic of plasma properties.

The lines are fit with single Gaussian functions and a local continuum generated within $\pm 1.0 \text{ \AA}$ of the line center. Except for Fe, the identifications indicate Lyman α emissions from H-like ions of Ne X, Mg XII, Si XIV, and S XVI. In the case of Fe there is Fe XXV, Fe XXVI, and possibly Fe XXIV. The Ne X is blended into a very broad blend ranging from 10.5 to 12.5 \AA which include also Fe XXIV and lower Fe transitions, and here we cannot readily isolate its line properties. The brightest lines are isolated we expect no significant blends. The line centroids appear slightly blue-shifted with respect to the expected rest wavelengths. This is anticipated due to Cyg X-2's systemic motion towards the Sun of $\sim 220 \text{ km s}^{-1}$ (Cowley et al. 1979). Table 2 summarizes the properties of the brightest emission lines, with the line wavelengths corrected for the systemic motion. The lines appear within less than $\sim 12 \text{ m\AA}$ of the rest wavelengths on average. The lines from Mg XII, Si XIV, S XVI and the Fe K region are most significant. Figure 2 shows the spectrum plus residuals near Fe K as well as three examples of the line significances on a velocity scale with respect to the rest wavelength. Doppler velocities deduced from the H/He-like lines range from 1100 at Fe XXVI to 2730 km s^{-1} at Mg XII. Also note that H-like line emissions generally contain two narrowly separated line components and we accounted for this separation in the calculation of the Doppler velocities. The Fe XXV appears wider because it is a line triplet and the widths of its line components are consistent with the other lines. The line width for Fe XXV in Table 2 was obtained by fitting a single function to the entire triplet. In Figure 2 we fixed the relative wavelengths to the respective resonance, intercombination, and forbidden line with line widths fixed to the value found for Fe XXVI. This shows that in Fe XXV the bulk of the line flux is associated with the intercombination line (strong green line).

The spectrum harbors some narrower emission lines as well at wavelengths below 8 \AA with line widths of several hundred km s^{-1} . Most significant is the one at 7.98 \AA which identifies with the shortest wavelength of the Fe XXIV (Li-like) ion sequence. The second strongest is the one at 7.80 \AA which consistent with a strong intercombination line of Al XII, with no detection of a resonance or forbidden line component. The detection of the Al XII intercombination line as well as the non-detection of the forbidden line provides a simple R ratio estimate. The R ratio is an important density diagnostic and is defined as the ratio of forbidden to intercombination line flux. Based on the continuum flux we can put an upper limit to the forbidden line flux to $2.3 \times 10^{-6} \text{ ph s}^{-1} \text{ cm}^{-2}$ leading to an upper limit of the R ratio of 0.06 with 90% confidence of 0.01. In the case of Fe XXV we can use the single fit components of the intercombination line ($1.2 \times 10^{-4} \text{ ph s}^{-1} \text{ cm}^{-2}$) and the forbidden line ($0.3 \times 10^{-4} \text{ ph s}^{-1} \text{ cm}^{-2}$) to estimate $R \sim 0.3$, well below unity.

5. LINE FLUXES ALONG THE Z-PATTERN

We also integrated the spectra along the three spectra branches. The time in the HB branch is about 15%, in the NB 30%, and in the FB is about 55% of the total exposure. The narrower lines at 7.98 \AA and 7.80 \AA were present in all branches with some variability. The broad Ne X line blend be-

tween 10.5 and 12.5 \AA is detected in all branches as well, but appears most prominent in the FB. Figure 3 shows the evolution of line fluxes of the brightest lines which are Mg XII, Si XIV, S XVI, and Fe XXV (see Table 2). Mg XII is hardly detected in the HB and NB, S XVI is very weak in the HB. The others are significant in all branches. The flux at Fe XXV increases by a factor 4, at Mg XII and S XVI by an order of magnitude from the HB to the FB. We emphasize that the observed variation pattern cannot be a result of the CTI grade losses, which would have yielded the opposite trend. Application of the grade loss rates would actually enhance this pattern.

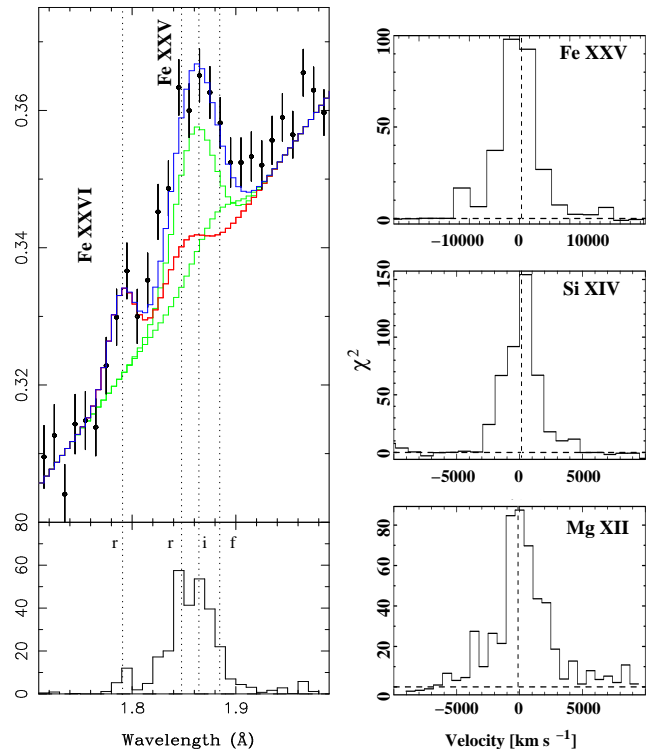


FIG. 2.— **Left:** Unfolded spectrum and residuals near the Fe K region. The blue line represents the full line model, the red line represents the resonance lines, the strong green line the intercombination, and the weak green line the forbidden line of Fe XXV. **Right:** Line residuals of Mg XII, Si XIV, and Fe XXV plotted on a velocity scale relative to the lines rest wavelengths.

The current lack of calibration in cc-mode does not allow us to apply yet more detailed models to determine the full ionization balance and its change from the HB to the NB. However by using the *photemis* function within the photoionization code XSTAR⁶ to determine relative line strengths we can set rough limits to the ionization parameter. We find that the detected line emissivities require ionization parameters $\log \xi$ of above 3. For the variation from the HB to the FB we expect changes from 2.8 to 3.4, mostly based on the ratio of Fe XXV to Fe XXVI.

6. ADC PROPERTIES IN Cyg X-2

The preliminary analysis of a long exposure of the bright Z-source Cyg X-2 presented in this letter produced a variety of new results. We detect a number of broad emission lines at short wavelengths corresponding to Ne X, Mg XII, Si XIV, S XVI, as well as Fe XXIV, Fe XXV, and Fe XXVI. The detections confirm the identifications from

⁶ see <http://heasarc.gsfc.nasa.gov/docs/software/xstar/xstar.h>

the *BBXRT*, *ASCA*, and *BeppoSAX* observations with respect to the Fe XXV and Fe L detections (Smale et al. 1994; Di Salvo et al. 2002) and emissions from other abundant elements (Kuulkers et al. 1997). For the first time we can directly determine physical properties of the ADC as well as true source luminosities along the Z-track. The emissivities indicate ionization parameters well above $\log \xi = 3$. Such high ionization parameters imply plasma temperatures in excess of 10^6 K.

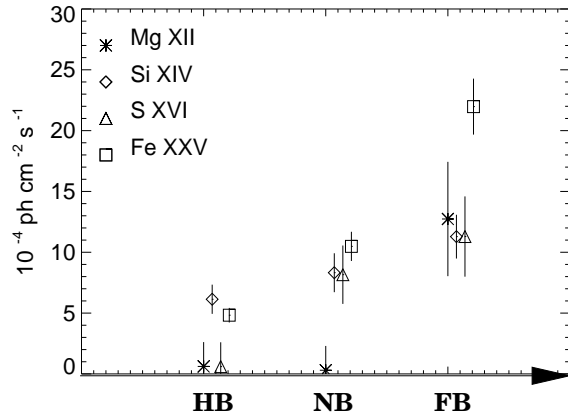


FIG. 3.— Line fluxes of the brightest and broadest lines as measured separately on the HB, NB, and FB.

We can use the line widths as well as the determined R ratios to determine the basic properties of the ADC in Cyg X-2. The lines are observed at rest and appear very broad with Doppler velocities between 1120 and 2730 km s⁻¹, which at an inclination of 60 degrees places the emissions at disk radii of $1.8 - 11.0 \times 10^9$ cm from the neutron star. These radii are consistent with recent model predictions for ADC sources (Jimenez-Garate et al. 2002) and specifically for Cyg X-2 by Church, Halai & Balucińska-Church (2006). Furthermore, in equilibrium and at the high temperatures the He-like density diagnostics of photoionized plasmas behaves kinetically identical to the collisional case (Liedahl 1999) and we can use our R ratio and the density dependence in the Astrophysi-

cal Plasma Emission Database⁷ (Smith et al. 2001) to determine a lower limit of $6.4(\pm 1.4) \times 10^{14}$ cm⁻³ to the density of the corona. In the case of the Fe XXV line APED does not provide the diagnostic, however its estimated R ratio of less than unity indicates densities beyond 10^{17} cm⁻³, which is the critical density for Fe XXV (Schulz et al. 2008). These densities are too high to allow for a direct view through this corona thus limiting the scale height above the accretion disk to well below 30 deg for an assumed inclination of 60 deg. Stationary ADCs with such scale heights have been modeled (Jimenez-Garate et al. 2002) and observed for sources like Her X-1, 4U 1822-37, and Cir X-1 (Cottam et al. 2001; Jimenez-Garate et al. 2005; Schulz et al. 2008).

At a radius of 10^{10} cm, an average ionization parameter of 2000, and an average density of 10^{15} cm⁻³ we estimate a luminosity of 2×10^{38} erg s⁻¹, consistent with the average source luminosity during our observations of $1.8 \times 10^{36} D^2 / [\text{kpc}]$ erg s⁻¹ at a source distance of 10.5 kpc.

For the first time we find substantial line flux variability along the Z-pattern. At coronal densities and radii as stated above, the implied change in ξ from ~ 2.8 to 3.4 provides us with an independent measure of the true change of the source luminosity along the Z-profile. The change in average heating luminosity is then from 0.63×10^{38} erg s⁻¹ ($0.35 \times L_{\text{Edd}}$) in the HB to 2.5×10^{38} erg s⁻¹ ($1.40 \times L_{\text{Edd}}$) in the FB. The direction of heating in such an ADC has immediate implications with respect to recently published Z-models (Church et al. 2008; Lin, Remillard & Homan 2008).

Future aspects of the analysis include a more detailed understanding of the various ionization regimes observed and their changes along the Z-track. The next step in the analysis thus is to fit the spectra with physical models to obtain the full range of ionization balances with specific attention to the complex line blend around 1 keV.

We thank all the members of the *Chandra* team for their enormous efforts. We gratefully acknowledge the financial support of Smithsonian Astrophysical Observatory contract SVI-61010 for the CXC.

⁷ see also [http://cxc.harvard.edu/atomdb/features\\$_density.html](http://cxc.harvard.edu/atomdb/features$_density.html)

REFERENCES

- Brandt, W.N. & Schulz, N.S. 2000, *ApJ*, 544, L123
 Canizares, C. R., Davis, J. E., Dewey, D., Flanagan, K. A., Galton, E. B., Huenemoerder, D. P., Ishibashi, K., Markert, T. H., Marshall, H. L., McGuirk, M., Schattenburg, M. L., Schulz, N. S., Smith, H. I., & Wise, M. 2005, *PASP*, 117, 1144
 Church, M. J., Halai, G. S., & Bałucińska-Church, M., *A&A*, 460, 233
 Church, M. J., Jackson, N. K., Bałucińska-Church, M., Chin, J. 2008, *A&A*, 8, 191
 Cottam, J., Sako, M., Kahn, S. M., Paerels, F., Liedahl, D. A. 2001, *ApJ*, 557, 101
 Cowley, A. P., Crampton, D., & Hutchings, J. B. 1979, *ApJ*, 231, 539
 Di Salvo, T., Farinelli, R., Burderi, L., Frontera, F., Kuulkers, E., Masetti, N., Robba, N. R., Stella, L., van der Klis, M. 2002, *A&A*, 386, 535
 Hasinger, G., van der Klis, M. 1989, *A&A*, 225, 79
 Hasinger, G., van der Klis, M., Ebisawa, K., Dotani, T. and Mitsuda, K. 1990, *A&A*, 235, 131
 Hirano, T., Hayakawa, S., Nagase, F., Masai, K. & Mitsuda, K. 1987, *PASJ*, 39, 619
 Houck, J. C. & Denicola, L. A. 2000, *ASP Conf. Ser.* 216: *Astronomical Data Analysis Software and Systems IX*, p. 591
 Jimenez-Garate, M. A., Raymond, J. C. & Liedahl, D. A. 2002, *ApJ*, 581, 1297
 Jimenez-Garate, M. A., Raymond, J. C., Liedahl, D. A., & Hailey, C. J. 2005, *ApJ*, 625, 931
 Juett, A. M., Schulz, N. S., & Chakrabarty, D. 2004, *ApJ*, 612, 308
 Kuulkers, E., Parmar, A. N., Owens, A., Oosterbroek, T., Lammers, U., 1997, *A&A*, 323, L29
 Lin, D., Remillard, R. A., Homan, J., 2008, *ApJ*, submitted
 Liedahl, D. A. 1999, in *Lecture Notes in Phys.* 520, *X-ray Spectroscopy in Astrophysics*, ed. J. van Paradijs & J. A. M. Bleeker (Berlin, Springer), pp. 189
 O'Brien, K., Horne, K., Gomer, R. H., Oke, J. B., and van der Klis, M. 2004, *MNRAS*, 350, 587
 Schulz, N. S.; Hasinger, G.; Trümper, J. 1989, *A&A*, 225, 48
 Schulz, N. S., Kallman, T. E., Galloway, D. K. & Brandt, W. N. 2008, *ApJ*, 676, 1091
 Smale, A. P., Done, C., Mushotzky, R. F. et al. 1993, *ApJ*, 410, 796
 Smale, A. P., Angelini, L., White, N. E., Mitsuda, K. and Dotani, T. 1994, *BAAS*, 26, 1484
 Smale, A. P. 1998, *ApJ*, 498, L141

- Smith, R. K., Brickhouse, N. S., Liedahl, D. A., Raymond, J. C., 2001, ApJ, 556, L91
- Vrtilek, S. D., Swank, J. H., Kelley, R. L. and Kahn, S. M. 1988, ApJ, 329, 276
- White, N. E., Peacock, A. & Taylor, B. G. 1985, ApJ, 296, 475
- White, N. E., Peacock, A., Hasinger, G., Mason, K. O., Manzo, G., Taylor, B. G. & Branduardi-Raymont, G. 1986, MNRAS, 218, 129
- Yao, Y., Schulz, N. S., Nowak, M. N., Canizares, C. R. 2008, ApJ, in press